J Neurophysiol 128: 1518–1533, 2022.
First published November 2, 2022; doi:10.1152/jn.00240.2022

american physiological society

JNP JOURNAL OF NEUROPHYSIOLOGY

RESEARCH ARTICLE

Control of Movement

Parietofrontal oscillations show hand-specific interactions with top-down movement plans

Gunnar Blohm,[1,2,3,5] Douglas O. Cheyne,[4] and J. Douglas Crawford[2,3,5]

[1]*Centre of Neuroscience Studies, Departments of Biomedical & Molecular Sciences, Mathematics & Statistics, and Psychology and School of Computing, Queen's University, Kingston, Ontario, Canada;* [2]*Centre for Vision Research, York University, Toronto, Ontario, Canada;* [3]*Canadian Action and Perception Network (CAPnet), Montreal, Quebec, Canada;* [4]*Program in Neurosciences and Mental Health, The Hospital for Sick Children Research Institute, Toronto, Ontario, Canada; and* [5]*Vision: Science to Applications (VISTA) program, Departments of Psychology, Biology, and Kinesiology and Health Sciences and Neuroscience Graduate Diploma Program, York University, Toronto, Ontario, Canada*

Abstract

To generate a hand-specific reach plan, the brain must integrate hand-specific signals with the desired movement strategy. Although various neurophysiology/imaging studies have investigated hand-target interactions in simple reach-to-target tasks, the whole brain timing and distribution of this process remain unclear, especially for more complex, instruction-dependent motor strategies. Previously, we showed that a pro/anti pointing instruction influences magnetoencephalographic (MEG) signals in frontal cortex that then propagate recurrently through parietal cortex (Blohm G, Alikhanian H, Gaetz W, Goltz HC, DeSouza JF, Cheyne DO, Crawford JD. *NeuroImage* 197: 306–319, 2019). Here, we contrasted left versus right hand pointing in the same task to investigate *1*) which cortical regions of interest show hand specificity and *2*) which of those areas interact with the instructed motor plan. Eight bilateral areas, the parietooccipital junction (POJ), superior parietooccipital cortex (SPOC), supramarginal gyrus (SMG), medial/anterior interparietal sulcus (mIPS/aIPS), primary somatosensory/motor cortex (S1/M1), and dorsal premotor cortex (PMd), showed hand-specific changes in beta band power, with four of these (M1, S1, SMG, aIPS) showing robust activation before movement onset. M1, SMG, SPOC, and aIPS showed significant interactions between contralateral hand specificity and the instructed motor plan but not with bottom-up target signals. Separate hand/motor signals emerged relatively early and lasted through execution, whereas hand-motor interactions only occurred close to movement onset. Taken together with our previous results, these findings show that instruction-dependent motor plans emerge in frontal cortex and interact recurrently with hand-specific parietofrontal signals before movement onset to produce hand-specific motor behaviors.

NEW & NOTEWORTHY The brain must generate different motor signals depending on which hand is used. The distribution and timing of hand use/instructed motor plan integration are not understood at the whole brain level. Using MEG we show that different action planning subnetworks code for hand usage and integrating hand use into a hand-specific motor plan. The timing indicates that frontal cortex first creates a general motor plan and then integrates hand specificity to produce a hand-specific motor plan.

arm movements; magnetoencephalography; movement planning; pointing; sensorimotor transformation

INTRODUCTION

Motor planning is a complex process that encompasses many sensorimotor computations, including sensory processing, target selection, reference frame transformations, and multisensory integration (1–3). Although each of these is an important process, ultimately, a motor plan must be executed using specific effectors (e.g., the eye, hand, or foot). Once an effector system is chosen (i.e., the hand), the brain must still choose which hand to use and which motor strategy to employ and then integrate these signals to produce a hand-specific motor plan. Various studies have investigated

Correspondence: G. Blohm (gunnar.blohm@queensu.ca).
Submitted 3 June 2022 / Revised 3 October 2022 / Accepted 20 October 2022

hand-target information for visually guided pointing/reaching (see below), but the temporal sequence and frequency dependence of this process remain unclear at the whole brain level, especially in the presence of "top-down," instruction-dependent motor strategies (4).

An early step in this process is effector selection (5), which in the parietofrontal reach system requires hand-specific signals (6). At the sensory input level (somatosensory cortex) there is clear contralateral hand representation, but after that one sees a mix of unilateral and bilateral signals, even down to the level of primary motor cortex (7–12). Human neuroimaging studies suggest that parietofrontal cortex is bilaterally activated by unilateral reaches, but with a preference for the contralateral limb (6, 13–21). Likewise, the monkey "parietal reach region" shows some ipsilateral signals (22) but is primarily modulated by, and causally related to, reaches of the contralateral limb (7, 23). Overall, these findings suggest a progression of ipsilateral and bilateral representations, but the whole brain distributions and timing of these signals remain unclear.

Furthermore, the presence of hand-specific information (left vs. right hand use, e.g., in somatosensory cortex) does not mean that this has been integrated into a motor plan. Such integration is necessary to activate motor commands for the correct hand, account for the correct initial hand position when calculating the extrinsic hand movement vector, and ultimately activate the correct intrinsic muscle synergies (which will tend to be opposite for opposite arms to produce the same horizontal motion in space) (24, 25). Most early sensorimotor studies have focused on the feedforward integration of visual target information with hand information to compute the reach vector (26, 27). This is thought to occur in parietal cortex (24, 28–35). However, it is not known how this occurs in more complex, instruction-dependent or abstract motor strategies (36, 37).

An example of an instruction-dependent motor strategy is the pro/anti reach task, where participants are instructed to point toward/away from a visual stimulus (14, 38–41). In our previous magnetoencephalography (MEG) study (42) we found that the pro/anti instruction first influences frontal cortex, in both alpha and beta bands, and then propagates this to more posterior cortical sites. It has been speculated that this might involve "mirroring" the reach goal, which would then require recalculating the reach vector relative to hand-specific signals (14, 40, 43). But again, it is not known how this strategy is integrated with hand-specific information to implement a specific reach command.

In the present study, we recorded MEG signals in the pro/anti pointing paradigm used in our previous study (42) but tested the left and right hands separately. This allowed us to derive both a hand specificity index and the instruction-dependent motor vector (42). We then performed a region of interest (ROI) analysis based on the areas identified in our previous study (44). We hypothesized that although many cortical areas might show hand-dependent modulation [e.g., primary motor (M1) and somatosensory (S1) cortex], only those involved in integrating hand information into the motor plan would show an interaction between hand specificity and extrinsic motor vector coding in their oscillatory activity. Furthermore, we hypothesized that a top-down motor instruction might require recalculation of the motor vector, thus requiring a specific progression toward an integrated "hand-plan" motor command. Our results confirm left versus right hand use specificity in various cortical areas and suggest a specific spatiotemporal progression from independent hand/motor signals to integrated hand-motor coding.

METHODS

We used MEG to obtain brain signals with high spatiotemporal resolution (45, 46) that could inform us about hand use and integration of hand information into movement plans. To achieve this, we asked participants to perform a pro/anti pointing task in the MEG, using the left and right hands in separate blocks of trials. We then coregistered MEG sensor locations to individual participants' heads by using an anatomical MRI recording. This allowed us to perform whole brain source reconstruction of MEG signals and infer the precise oscillatory activity at specific previously uncovered brain regions involved in the task (44). We then compared this activity across trial types, left/right targets/movements, and the use of left and right hands to see which brain areas differentially synchronize or desynchronize with respect to which hand is used. These procedures are described in detail below. The data set, experimental conditions, and most of the analysis pipeline have been described and partially published previously (42, 44).

Participants

We recruited 10 participants for a pro/anti pointing experiment after written informed consent, 9 of whom performed the task with both hands (7 males, 2 females, 22–45 yr old; see *Statistical Analysis* for details about study design and power) and were included in this study. Of the nine included participants performing the task with both hands, eight reported themselves to have a right hand preference and one reported themself to have a left hand preference. We screened participants to ensure that none had any history of neurological dysfunction, injury, or metallic implants, and all (except 1 with amblyopia) participants had normal or corrected to normal vision. All procedures were approved by the York University and Hospital for Sick Children Ethics Boards.

Task

Participants performed pro and anti pointing movements in four separate sets of trials; two of those sets were left- and right-hand wrist pointing movements, respectively, with the forearm in the pronated posture. Each set of trials was composed of 100 trials for each of four balanced conditions: combinations of target left/right and pro/anti instruction for a total of 400 trials. Figure 1 shows the experimental task. Trials started with a fixation cross, followed by a 200-ms combined spatial/task cue presentation (Fig. 1*A*). Cues could appear 5 or 10 cm left or right of fixation (we averaged across eccentricities in the analysis) and were either green or red, indicating pro or anti conditions (color-task associations counterbalanced across participants). Fifteen hundred milliseconds after cue presentation, the fixation cross was dimmed, indicating to participants to make a wrist pointing

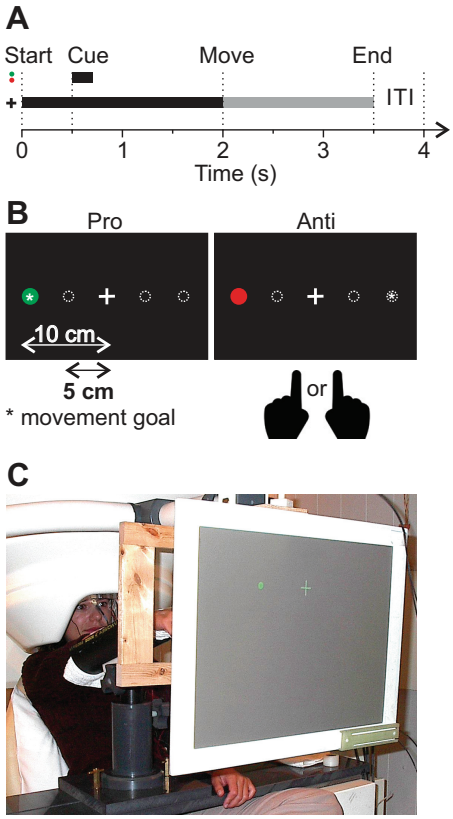

Figure 1. Experimental protocol. *A*: timeline of experiment. At the beginning of the trial, a central fixation cross appeared. Five hundred milliseconds later, a 200-ms cue (red or green) was briefly presented at 1 of 4 locations, 5 or 10 cm left or right of the fixation cross on the 1-m-distant screen. After another 1,300-ms delay, the fixation cross dimmed to indicate to participants to move and point their index finger to the goal location. Participants had 1,500 ms to complete this movement, followed by a 500-ms intertrial interval (ITI) during which the fixation cross disappeared. *B*: spatial setup on screen. Dotted circles are potential cue locations. Exemplary pro and anti conditions are shown. In anti trials the movement goal (asterisk) was at the mirror opposite location of the cue. Pointing movements were performed with the left or right hand in separate blocks of trials. *C*: picture of the experimental setup with forearm rest and display screen. The wooden frame held light barriers used for measuring movement direction.

movement toward (pro) or to the mirror opposite location of (anti) the cue.

Setup

Participants sat upright in the MEG apparatus (151-channel, axial gradiometers, 5-cm baseline, CTF MEG system, VSM Medtech, Coquitlam, BC, Canada, at the Toronto Hospital for Sick Children) in front of a 1-m-distant tangential screen with their head in the dewar and their forearm supported to reduce EMG artifacts (see Fig. 1*C*). The MEG was located in a magnetically shielded room (Vacuumschmelze Ak3b). Noise levels were below 10 fT/$\sqrt{}$Hz above 1.0 Hz. MEG data were online low-pass filtered at 200 Hz with synthetic third-order gradiometer noise cancelation. Bipolar temporal electrooculographic (EOG) and forearm electromyographic (EMG) signals were recorded simultaneously with MEG signals (at 625 Hz) to control for fixation and measure wrist movement onset. We used Ag/AgCl solid gel Neuroline (Ambu) electrodes of type 715 12-U/C. Pairs of EMG electrodes were placed over extensor carpi radialis longus (ECRL), extensor communis digitorum (ECD), extensor carpi ulnaris (ECU), and supinator longus (SL) muscles. Participants' arm was immobilized by an adjustable forearm rest so that pointing could be performed through wrist movements to align the index finger with the intended location on the screen. In addition to EMG, we also used light barriers that the finger passed when pointing as an additional, independent measure of movement direction (see Fig. 1*C*).

Visual stimuli were rear-projected (Sanyo PLC-XP51 LCD projector with Navitar model 829MCZ087 zoom lens) at 60 Hz onto a translucent screen (Fig. 1*C*) with Presentation (Neurobehavioral Systems, Inc., Albany, CA), and timing signals were recorded by the MEG hardware through parallel port interfacing. Participants were outfitted with fiducial head localization coils, and head position in the MEG was acquired at the beginning and end of each scan. Before or after MEG recordings, we obtained structural [T1-weighted, 3-dimensional (3-D)-SPGR] MRI scans from a 1.5-T Signa Advantage System (GE Medical Systems, Milwaukee, WI), including the fiducial locations for coregistration of MEG signals with brain coordinates (see below; Table 1). For each participant we used the T1-weighted MR data and the BrainSuite software package (47) to derive the inner skull surface.

Analysis

All analyses were done in MATLAB (The MathWorks, Inc., Natick, MA). To detect movement onset, we first band-pass

Table 1. *Average Talairach coordinates of functional brain areas*

Brain Area	Left Hemisphere	Right Hemisphere	References
V1/2	−8, −91, 0	7, −89, 1	(50)
V3/V3a	−21, −85, 16	20, −87, 15	(50, 51)
SPOC	−9, −71, 37	10, −77, 34	(52)
AG	−35, −61, 35	32, −70, 35	(52)
POJ	−18, −79, 43	16, −79, 43	(21)
mIPS	−23, −54, 46	27, −55, 49	(48, 53)
pIPS	−22, −61, 40	23, −62, 40	(54)
aIPS	−37, −40, 44	37, −44, 47	(48, 55)
SMG	−43, −35, 49	41, −41, 39	(48, 54)
STS	−45, −57, 15	49, −41, 12	(56)
S1	−40, −26, 48	39, −26, 40	(57)
M1	−35, −23, 54	37, −23, 52	(57)
SMA	−4, −9, 52	3, −7, 49	(57)
PMd	−27, −14, 61	21, −14, 61	(57, 58)
FEF	−28, −1, 43	31, −2, 45	(59)
PMv	−50, 5, 21	48, 8, 21	(57)

Values are average Talairach coordinates (in mm) of functional brain areas. Activation regions of interest were identified with an adaptive clustering approach (44) and cross-validated from the literature (indicated by references). We focused on sites corresponding to visual areas V1/2 and V3/3a, superior parietal occipital cortex (SPOC), angular gyrus (AG), parietal occipital junction (POJ), medial intraparietal sulcus (mIPS), posterior intraparietal sulcus (pIPS), anterior intraparietal sulcus (aIPS), supramarginal gyrus (SMG), superior temporal sulcus (STS), primary somatosensory cortex, (S1), primary motor cortex (M1), supplementary motor area (SMA), frontal eye fields (FEF), and dorsal and ventral premotor cortex (PMd and PMv). Note that compared with our previous studies (42, 44) we updated the names of mIPS, aIPS, SMG, and pIPS to bring our nomenclature in line with the most recent literature in this area (48, 49).

filtered EMG data between 15 Hz and 200 Hz and full-wave rectified it. Then we used an algorithm to automatically detect when EMG signals exceeded 3 standard deviations of baseline activity (measured before target cue onset). The first detection time across all four muscles was taken as movement onset time and visually inspected and manually corrected if necessary (<2% of trials). All data were then aligned to both cue onset (−500 ms to 1,500 ms around cue onset) and movement onset (−1,500 ms to 500 ms around movement onset) and extracted for further analysis. Trials with movement direction errors were discarded from further analysis (3.2% of total trials across participants). Movement errors were defined as movements going into the wrong direction, i.e., opposite to the pro trial cue or toward the anti trial cue. We did not allow for corrective movement, i.e., when the initial movement direction was erroneous despite later corrections, the trial was tagged as an error trial and discarded. The directions of all movements (including direction errors) were confirmed by the light barriers signaling that fingers interrupted the light beam when crossing the light barrier.

We performed MEG source reconstruction using a scalar (zero noise gain) minimum-variance beamformer algorithm (60–63) implemented in the Brainwave MATLAB toolbox (64) and additional custom code. This inverse method has been shown to achieve high localization accuracy under conditions of low to moderate signal-to-noise ratio (SNR) (65, 66). All further analyses were conducted in source space. We focused on previously reported independently identified regions of interest (ROIs) from the same data set (42, 44); briefly, we used adaptive clustering on peak whole brain activations in time-averaged raw, noncontrasted data to identify reliable clusters of brain activation and determined area labels that most likely corresponded to the clusters from the literature (see references in Table 1). Note that using the raw, noncontrasted data for determining ROIs was an orthogonal approach to our condition-contrasted analyses, making this a statistically valid approach (67, 68). We then used the beamformer to extract estimated source time courses of oscillatory activity for each trial at the ROI locations (see Table 1). We used those individual trial data to compute time-frequency responses (TFRs) at those ROIs with standard wavelet transforms. For spatial averaging across participants, individual participants' source activity was transformed into MNI coordinate space with standard affine transformations (linear and nonlinear warping) in SPM 8 and then projected onto a surface mesh of an average brain [PALS-B12 atlas (69)] with Caret (70).

As in our previous study (42), our analysis took advantage of the spatial lateralization of information processing in the brain (e.g., Ref. 71) to highlight our dependent variables and negate irrelevant variables. Therefore, where applicable, we averaged or subtracted right from left targets, right from left movements, right from left hand use, and/or right from left cortical activation (signal power in a frequency band of interest) for a given brain region. This is in line with what has previously been done in recent neurophysiology (41) and neuroimaging (14, 42, 72) anti reach studies. We then used these contrasts to highlight specificity with respect to which hand was used, whether sensory processing or movement processing dominated, and whether sensory/motor processing signals were modulated by which hand was used (we call this the hand-sensory/motor code interaction effect).

Since M1 is expected to show strongly lateralized hand effects and motor commands, we used this as a test case to develop our specific analysis pipelines and then applied these pipelines to our other brain areas (see RESULTS). In the case of hand-specific coding, we confirmed that for a given region and hand the change in oscillatory power was largely independent of target/movement direction (Fig. 2*A*) and pro/anti instruction (Fig. 2*B*), so we averaged across these parameters (Fig. 2, *right*). Note that this had no influence on hand effects (see RESULTS) except double the statistical power of our data. We then subtracted the average activity across all conditions in Left Hand from Right Hand to obtain a single hand main effect for each brain area:

$$\text{Hand effect} = \text{Left Hand}_{\text{L+R/pro+anti}} - \text{Right Hand}_{\text{L+R/pro+anti}}$$

where L/R stands for left/right target location.

Finally, in some cases we subtracted left brain from right brain data for each region of interest, to obtain a single bilateral measure of hand effect. The latter parts of this pipeline are summarized in RESULTS (Fig. 3).

To investigate the interaction effect between hand use and motor coding we first computed the spatial motor code for a given hand used, as in our previous study (42):

$$\text{Motor Code} = (\text{StimL}_{\text{pro}} + \text{StimR}_{\text{anti}}) - (\text{StimL}_{\text{anti}} + \text{StimR}_{\text{pro}})$$

where StimL/StimR correspond to the left and tight sensory cues. Thus, the motor code relies on the fact that the same movement results from a left cue in the pro condition and a right cue in the anti condition and vice versa. Note that this procedure is designed to identify a high-level extrinsic spatial code; the motor system must ultimately convert this to hand-specific intrinsic muscle codes (73).

If motor coding dominated an area's activation pattern, then we expect any trials leading to the same movement to

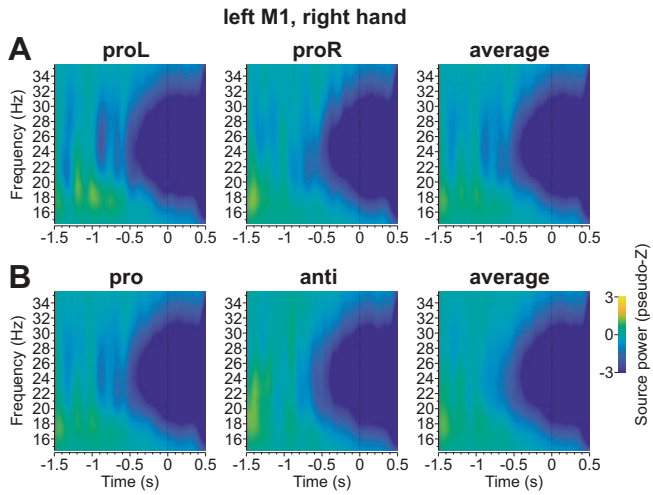

Figure 2. Left/right and pro/anti desynchronization in M1. *Left* and *center*: time-frequency responses (TFR) for beta-band activity (15–35 Hz) are shown for right hand conditions in left M1, averaged across all participants. *Right*: the average across left and right target/movement directions (*A*) and pro/anti instruction trials (*B*). *Time 0* indicates movement onset.

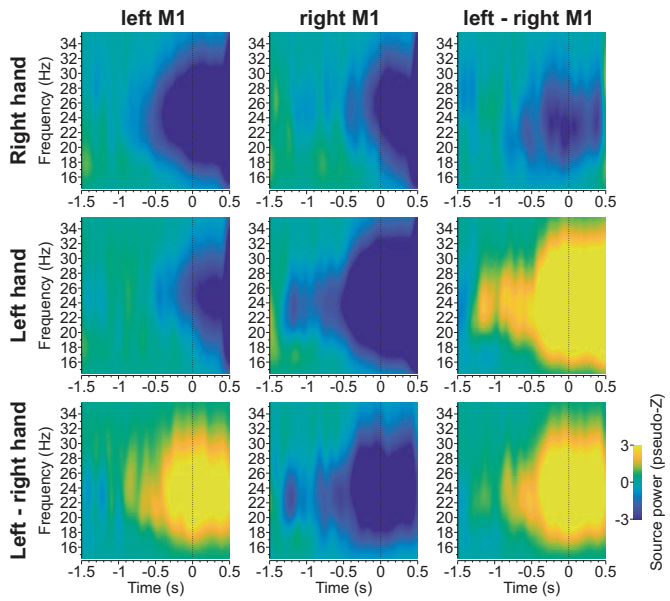

Figure 3. Subtraction logic leading to single bilateral site-specific hand coding index for M1. Each panel shows the oscillatory power change with respect to baseline, averaged across all task conditions (pro/anti, left/right cue) and plotted as a function of time (where 0 = movement onset). *Left*: activity for left M1. *Center*: activity for right M1. *Right*: the differential activity between right and left M1. *Top*: right hand activity. *Middle*: left hand activity. *Bottom*: the differential activity between right and left hand. The differential activity across sites shows how for a given hand (rows) left and right M1 differentially code for hand information. Conversely, differential activity across hand usage shows how for a given lateralized brain site (columns) the activity differs between left and right hand usage.

result in similar brain activation; opposite movements should lead to opposite activity patterns, e.g., desynchronization versus resynchronization.

To obtain the interaction between this motor code and hand specificity, we performed the following subtraction:

$$\text{Hand} - \text{Motor Coding Interaction} = \text{Motor Code}_{\text{Left Hand}} - \text{Motor Code}_{\text{Right Hand}}$$

A significant hand-motor coding interaction effect means that the motor code is different depending on which hand is used, indicating integration of hand choice into the movement plan. Conversely, no difference would indicate that the motor code is independent of which hand will be used.

We also computed a sensory code using similar principles (42) highlighting the differential activation of left versus right targets irrespective of movement direction and tested its interaction with hand specificity:

$$\text{Hand} - \text{Sensory Coding Interaction} = \text{Sensory Code}_{\text{Left Hand}} - \text{Sensory Code}_{\text{Right Hand}}$$

with Sensory Code = $(\text{StimL}_{\text{pro}} + \text{StimL}_{\text{anti}}) - (\text{StimR}_{\text{pro}} + \text{StimR}_{\text{anti}})$. However, these results were never significant and are not reported below.

Statistical Analysis

Reach studies yield highly robust neuroimaging data and thus tend to employ fewer participants than perceptual or cognitive studies (14, 42). In our design, we further offset participant numbers by compensating the low number of participants with a very high number of trials per participant (74), e.g., all hand main effect and hand-motor code interaction effect computations relied on the use of ~800 trials/participant. Statistical significance for individual ROI time series was determined when baseline-subtracted source power across participants for a given frequency band was consistently different from zero for at least consecutive 100 ms [temporal clustering (75)]. We used a two-sided *t* test to check for significance ($\alpha = 0.05$). Post hoc power analysis (G*Power) indicated power >0.5 (uncorrected for multiple comparisons) for alpha- and beta-band results in all ROIs, consistent with the standards reported in Ref. 74. Only ROIs that met this criterion are reported below. Note that we did not perform statistical testing for whole brain averages, as those had been used to identify the ROIs in the first place through adaptive clustering (44). Also, adaptive clustering used the raw, noncontrasted, time-averaged whole brain activations, and this procedure thus provided independent, orthogonal results to our condition-contrasted analysis here; this prevented double-dipping (67, 68). Thus, the whole brain projections are for visualization only.

RESULTS

Overview and Predictions

We tested 16 bilateral ROIs (see METHODS, Table 1) thought to be involved in the sensorimotor aspects of reach planning. Specifically, we investigated visual areas V1/V2 and V3/V3a, superior parietal occipital cortex (SPOC), angular gyrus (AG), parietal occipital junction (POJ), posterior intraparietal sulcus (pIPS), medial intraparietal sulcus (mIPS), anterior intraparietal sulcus (aIPS), supramarginal gyrus (SMG), superior temporal sulcus (STS), primary somatosensory cortex (S1), primary motor cortex (M1), supplementary motor area (SMA), frontal eye fields (FEF), and dorsal and ventral premotor cortex (PMd and PMv). We henceforth use the terms "sites" to refer to the specific coordinates of these ROIs and "areas" for the surrounding regions.

As noted above, we previously showed that during the pro/anti reach task this network of sites/areas first propagates feedforward sensory information (target direction independent of movement direction) from occipital to frontal areas. Sensory coding is present when brain activity patterns for right cue locations are different from left cue locations, but pro and anti conditions do not differ for a given cue location. Next, the instruction-dependent movement plan (movement direction independent of target direction) emerges as the same activity pattern for left cue pro and right cue anti conditions (and vice versa) because they result in the same final leftward (resp. rightward) movement. This instruction-dependent movement plan progressively dominates network activity in a front-to-back progression until movement onset (42). This progression was observed in both the alpha and beta bands, so the same bands were investigated here. For the present study we investigated both sensory and motor code interactions with hand position but did not find significant hand-sensory interactions, so only hand-motor interactions are reported below.

Specifically, we describe first the main effect of hand use on our sites/areas and then the interaction of the movement

plan (independent of target direction) with hand use to produce an integrated "hand-plan" movement command (5). To describe hand specificity, we show contrasts of event-related activity when the left versus the right hand was used while averaging across all stimulus conditions (left/right cue, pro/anti trials). We predicted that early hand sensory areas (S1) and late motor areas (M1) would show hand specificity and asked which intermediate high-level sensorimotor areas would show the same. To investigate the interaction between hand specificity and the top-down motor code we simply subtracted the right hand motor code from the left hand motor code. We predicted that only late (i.e., after S1) hand-specific areas would also show hand-plan motor interactions, including areas that might normally be involved in hand choice for specific tasks and hand-specific conversions from extrinsic to intrinsic muscle coordinates (73). Specific results are described below.

Hand Main Effect

Figure 3 shows the later stages of our analysis pipeline (after direction and instruction averaging, see METHODS) and main result for one example site (M1). M1 is shown here as a site that can be "safely" expected to show contralateral hand dominance, if our method works. Beta band-related power changes were averaged across all trials and plotted as a function of time, aligned at the point of movement onset (similar alpha band results are summarized below). Note that in this first analysis trials with left/right targets and pro/anti pointing instruction were pooled (~400 trials/hand/participant). The data were first plotted separately for the left/right hand (Fig. 3, *top* and *middle*) and left/right M1 (Fig. 3, *left* and *center*), corresponding to the four top left panels in Fig. 3. Note that lower power (desynchronization, shown as dark blue areas) is associated with increased neural activity (76). Planning-related power modulations appear to emerge ~1–0.5 s before movement onset (0 on the *x*-axis).

To isolate the hand effect and extract a single hand main effect for each site, we subtracted right hand trials from left hand trials (Fig. 3, *bottom*), resulting in what we called the hand main effect. Here (in Fig. 3, *bottom left* and *bottom center*) yellow signifies more activation for the left hand, and dark blue signifies more activation for the right hand. Finally, we subtracted the left brain from right brain data (Fig. 3, *right*) to obtain a single measure of bilateral hand specificity for each region (in this case M1). For the top two rows in Fig. 3, this subtraction results in the differential activation of left and right M1 separately for the right hand and the left hand. For example, the top row in Fig. 3 shows that planning to move the right hand leads to stronger desynchronization of left M1 than right M1, as expected. This observation is reversed for planning to move the left hand (middle row of Fig. 3). For the bottom row of Fig. 3, the combined subtraction [Left M1 (left − right hand) − Right M1 (left − right hand)] (Fig. 3, *bottom right*) summarizes the overall lateralization of the bilateral structure, where yellow indicates contralateral hand sensitivity. This highlights the expected lateralization of hand coding in M1, with relative left hand modulations in right M1 and right hand modulations in left M1. In other words, the positive result in the combined subtraction indicates a contralateral hand coding scheme (i.e., right hand in left M1, left hand in right M1) as one would expect.

We performed the same beta-band analysis on all 16 bilateral pairs of our selected brain sites (Table 1). Of these, we found significant hand-specific activity in eight bilateral pairs: POJ, SMG, S1, mIPS, SPOC, aIPS, M1, and PMd. The data were generally equal and opposite between bilateral pairs (see Supplemental Fig. S1; all Supplemental Materials are available at https://doi.org/10.6084/m9.figshare.19962224), yielding summated power in the final bilateral subtraction (illustrated by the 8 panels in Fig. 4). Although each area showed significant hand-specific activation changes before movement, they showed area-specific activity patterns. Some sites (M1, S1, IPS, aIPS, PMd) showed relatively well-organized band-time patterns. These areas showed a strong positive subtraction (yellow in Fig. 4) indicating contralateral hand preference. Other areas showed intermediate (mIPS) or relatively weak (SPOC, POJ) patterns. In the latter cases, the onset of hand specificity

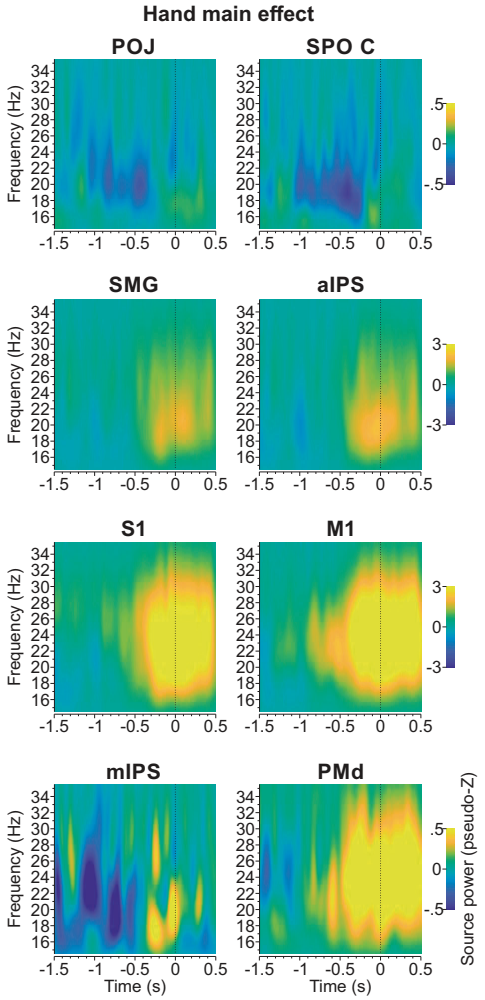

Figure 4. Hand main effect analysis for beta-band activity. Each panel contains temporal plots of activity changes from baseline, averaged across all task conditions. Only shown are the 8 regions that showed significant activation in the overall contrasts between right/left hand and left/right hemispheres, computed in the same way as Fig. 3, *bottom right*. aIPS, anterior interparietal sulcus; M1, primary motor cortex; mIPS, middle interparietal sulcus; PMd, dorsal premotor cortex; POJ, parietooccipital junction; S1, primary somatosensory cortex; SMG, supramarginal gyrus; SPOC, superior parietooccipital cortex.

is not clear from visual inspection of these plots, requiring further quantification (we return to this point below).

To visualize these patterns across the entire cortex, we computed average hand-specific beta activity changes from baseline (averaged across conditions) during the last 500-ms window preceding movement onset. The result of this analysis is shown in Fig. 5 for the left hand (Fig. 5, *left*) and the right hand (Fig. 5, *center*) separately. (In this case, we removed the left − right hand and left − right brain subtractions, so that whole brain results and their hand lateralization patterns can be viewed.) This shows that before movement onset there were widespread changes in oscillatory beta-band power across the cortex, with the suggestion of hand lateralization in some sites. To highlight this lateralization, we then subtracted right from left hand average activity patterns (Fig. 5, *right*). Since negative power is indicative of increasing neural activity, a positive result (orange in Fig. 5) signifies right hand preference and a negative result (blue) signifies left hand preference. The result shows strong hand-specific lateralization spanning dorsolateral parietofrontal cortex, with right hand preference in left cortex and left hand preference in right cortex. This pattern extended slightly more posterior on the left hemisphere (just ahead of our AG/pIPS, right mIPS coordinates) and forward toward bilateral prefrontal cortex (∼left/right PMv, FEF).

Figure 6 summarizes these observations and extends them both to the alpha band and to the temporal domain. Since the left and right hemispheres show opposite hand lateralization, it would not be appropriate to average them. Instead, we collapsed data across the left and right hemisphere data using a bilateral hemisphere subtraction and then extracted the 10 Hz (alpha) and 20 Hz (beta) frequencies from the last 500 ms before movement onset to generate plots in cortical space (Fig. 6, *top*): positive results (red/orange) indicate significant contralateral hand preference. These anatomic plots show peak hand specificity (yellow) in central regions (mIPS, aIPS, S1, M1) with lesser but still significant activation (orange) in surrounding areas (SMG, mIPS, PMd). Overall, beta modulations (Fig. 6, *right*) showed similar patterns of contralateral hand preference but were more widespread and pronounced compared with alpha modulations (Fig. 6, *left*). There were also frequency-dependent regional differences: for example, power changes related to hand-specific IPS modulations extended more posterior toward AG in the alpha band compared with the beta band, and beta activation extended further into prefrontal cortex.

Figure 6, *bottom* shows temporal plots of power in the alpha and beta bands for our sites of interest, again aligned on movement onset, where red indicates a significant deviation from equal hand specificity and a positive deflection indicates contralateral hand specificity. Sites that showed significant contralateral preference typically did so ∼1–0.5 s before movement onset (*time 0*). SMG, aIPS, S1, and M1 then showed a consistent buildup of significant contralateral hand specificity in both frequency bands during motor planning and execution. PMd showed a similar pattern, but only in the beta band. mIPS showed this pattern in the alpha band but did not reach significance. Otherwise, mIPS and SPOC/POJ activation (which was too small to show up in the anatomic plot) showed oscillations that only transiently reached significance and in the negative (ipsilateral hand) direction. No significant activations were found in sites V1, V2, V3/3a, AG, pIPS, STS, SMA, and PMv. Overall, SMG, aIPS, S1, and M1 showed the clearest specificity for the contralateral hand in the premotor planning phase of the task.

Hand-Motor Coding Interaction Effect

We previously found that before movement onset many parietal and frontal areas displayed coding of the movement

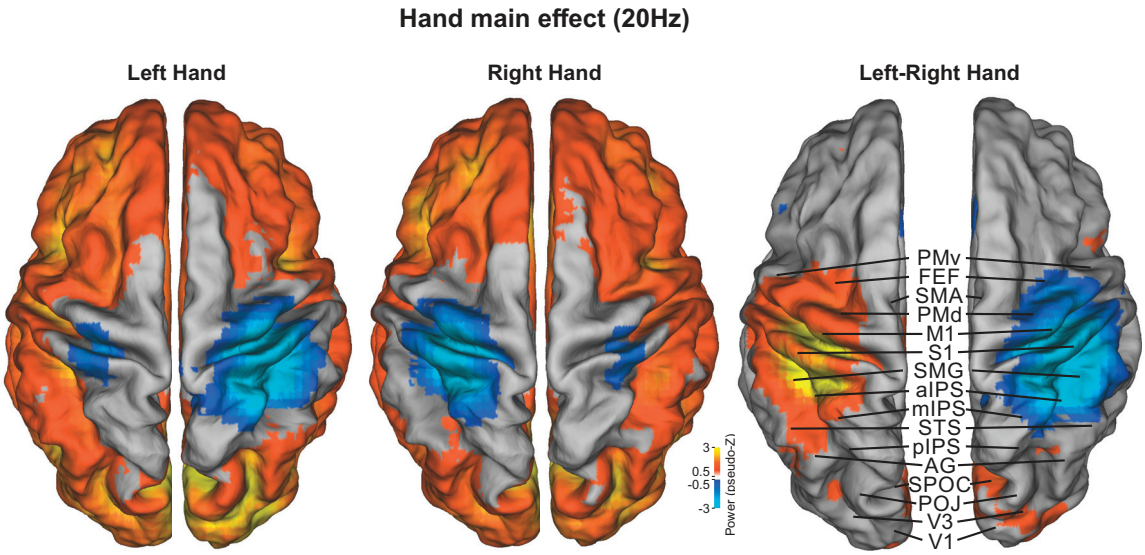

Figure 5. Average movement-aligned activities for each hand and hand main effect (left − right hand subtraction) across cortex. Beta-band activity change compared to pretask baseline was averaged for the last 500 ms before movement onset. Subtraction between right and left hand activity (*right*) highlights the hand-specific change in oscillatory power across the cortical surface. AG, angular gyrus; aIPS, anterior interparietal sulcus; FEF, frontal eye fields; M1, primary motor cortex; mIPS, medial interparietal sulcus; pIPS, posterior interparietal sulcus; PMd, dorsal premotor cortex; PMv, ventral premotor cortex; POJ, parietooccipital junction; S1, primary somatosensory cortex; SMA, supplementary motor area; SMG, supramarginal gyrus; SPOC, superior parietooccipital cortex; STS, superior temporal sulcus.

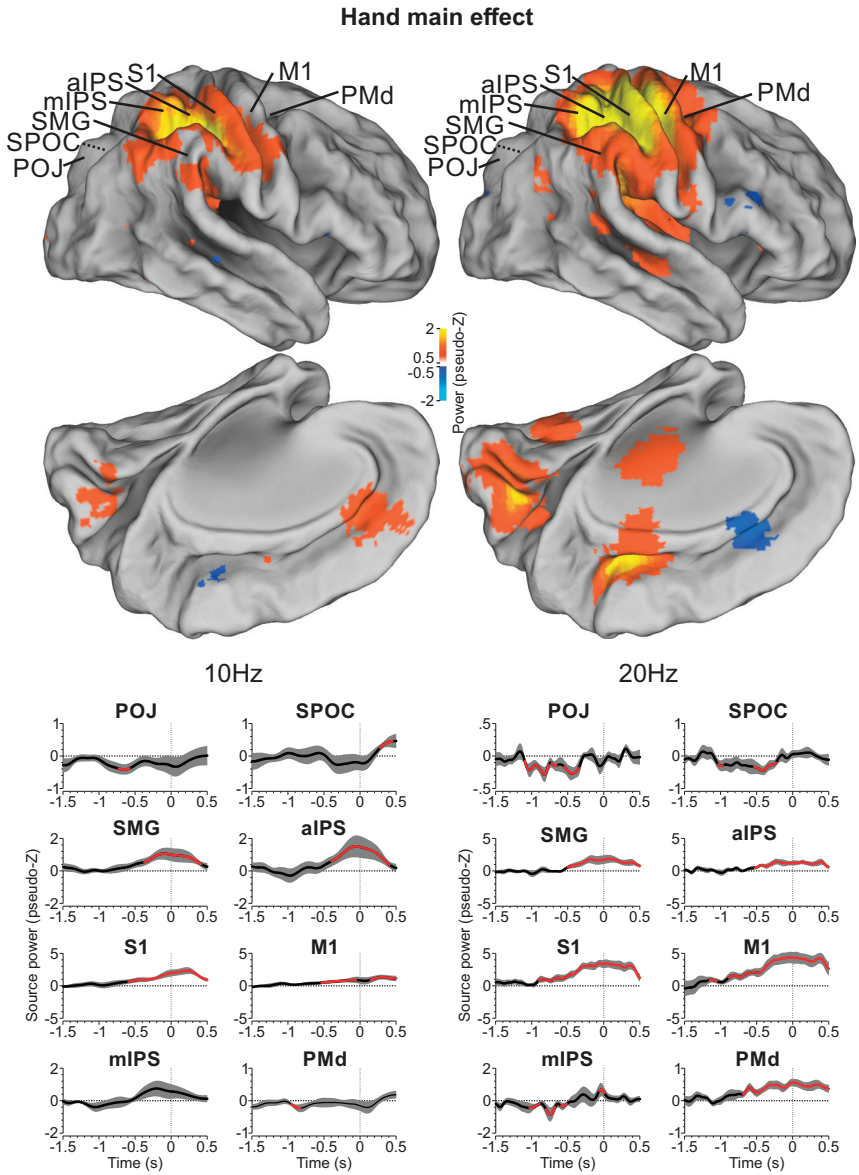

Figure 6. Spatial and temporal specificity of hand main effect in alpha and beta bands. *Top*: whole brain cortical pattern (1st row: lateral view; 2nd row: mesial view) associated with hand specificity averaged during the 500 ms before movement onset and projected onto the right cortical hemisphere (20 Hz data are the same as Fig. 5, *right*). *Bottom*: time courses of frequency power (10 Hz, *left*; 20 Hz, *right*) for active brain regions before and around movement onset (time 0 ms). Black shows mean signal across participants, gray area is the 95% confidence interval, and red indicates significant difference from 0. aIPS, anterior interparietal sulcus; M1, primary motor cortex; mIPS, medial interparietal sulcus; PMd, dorsal premotor cortex; POJ, parietooccipital junction; S1, primary somatosensory cortex; SMG, supramarginal gyrus; SPOC, superior parietooccipital cortex.

plan (see METHODS and Ref. 42). Specifically, we showed a main effect of motor coding in the same data set for POJ, SPOC, SMG, aIPS, S1, and M1 but not for mIPS (42). These motor codes were obtained by subtracting data from pro pointing and anti pointing trials (pooled in the hand analysis above) such that the directionality of the sensory stimuli cancels whereas the target and instruction-dependent motor directions summate (14, 42). In other words, this subtraction provides the instruction-dependent movement specificity of the area independent of visual stimulus location.

In *Hand Main Effect*, we show that a subset of those movement-tuned areas also show a main effect for coding of hand selectivity (Figs. 3–6), but this does not necessarily mean that this hand information is actually integrated into the motor plan. Here, we tested each of our relevant sites for an interaction effect between the main hand coding effect (described above) and motor coding (obtained in the same way as Ref. 42; see METHODS), i.e., whether there is a hand-specific motor code.

Figure 7 shows the steps taken in this analysis and the main result, again using M1 as our example site. This figure follows the same steps and logic as Fig. 3, except now we are looking at the power of the interaction between the hand effect and the motor code. In the first step, the motor code was computed separately for the left and right hand and left and right M1 (creating the 4 panels in the top left quadrant of Fig. 7). We then subtracted the left − right M1 to get the hemispheric difference (right panels of top 2 rows of Fig. 7) and hand difference (bottom panels of left 2 columns of Fig. 7) in the motor code. Similar to the hand main effect, these subtractions produced roughly opposite patterns of oscillatory power changes, (i.e., top right vs. middle right and bottom left vs. bottom center in Fig. 7). This suggests that the hand-motor plan is both hand specific and oppositely lateralized (anatomically). Combining both subtractions (Fig. 7, *bottom right*) produced a single hand-motor plan interaction index for bilateral M1. The significant negative deflection (blue) shown here provides a visual benchmark for what data

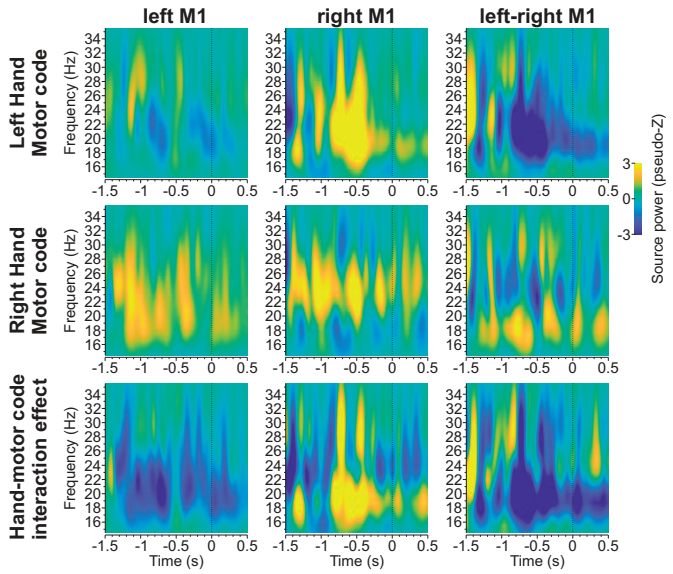

Figure 7. Hand-motor code interaction effect for M1 beta-band activity. Time-frequency response plots are shown separately for left hand motor coding (*top*), right hand motor coding (*middle*), and the difference between left and right motor coding (*bottom*) showing the interaction effect for left M1 (*left*), right M1 (*center*), and the left/right M1 contrast (*right*).

should look like if a site shows a motor plan specific to the contralateral hand, in other words, an integrated hand-motor plan.

Figure 8 shows the result of this beta-band analysis for the eight bilateral pairs that showed significant hand effects in our previous analysis. Again, blue (desynchronization) corresponds to the expected interaction resulting from both contralateral movement and contralateral hand coding, whereas yellow would denote an opposite interaction, e.g., ipsilateral hand for contralateral motor coding or contralateral hand for ipsilateral motor coding. Note that desynchronization in the interaction effect could also arise from ipsilateral hand and ipsilateral motor coding. Some sites showed a strong interaction in the expected direction (e.g., M1, SMG), others appear to show a mix of positive (blue) and negative (yellow) interactions depending on time and frequency band (SPOC, mIPS, aIPS, S1), and other sites show little or no hand-motor plan interaction effect at all (e.g., POJ, PMd). Of the sites that showed a significant interaction, only SMG, aIPS, and M1 showed clear interaction effects in the 500-ms period preceding action, with stronger motor coding for the contralateral hand (SPOC also showed some interaction, but this was a preference for motor coding in the ipsilateral hand). The other sites did not reach significance. (see Supplemental Fig. S2 for corresponding lateralized analysis results). Overall, these results suggest that SMG, aIPS, PMd, and possibly SPOC are involved in effector-motor plan integration in the premotor period, relatively lateralized for the opposite hand.

Figure 9 shows the functional anatomy and time courses of these interactions in our specific sites, collapsing across hemispheres as done in Fig. 6. Figure 9, *top*, shows desynchronization related to the interaction effect for 10 Hz (Fig. 9, *top left*) and 20 Hz (Fig. 9, *top right*) across the whole brain during the last 500-ms time window before movement onset. The beta band shows a broad swath of blue (contralateral hand/motor plan interaction), spanning aIPS, SMG, and M1 and with several other outlying sites. In contrast, in the alpha band only a small area in posterior parietal cortex showed desynchronization. In short, the hand-motor interaction was primarily observed in the beta band.

Figure 9, *bottom*, shows a more detailed look at the time course of the interaction effect in both frequency bands, where significant deviations from zero are indicated in red. Consistent with statements above, the alpha band showed very little significant interaction except for a few very brief "blips" before (PMd), during (POJ, S1), or after (SPOC) the planning stage. In the beta band, aIPS, SMG, and M1 showed significant interactions during the delay period. Interestingly, SPOC showed opposite interactions in the alpha and beta bands and during the movement; this was expected for contralateral motor coding since SPOC showed ipsilateral hand main effects (see Figs. 4 and 6). But overall, SPOC, SMG, aIPS, and M1 showed clear, hemispherically lateralized hand-motor interactions at various points of the planning phase for movement.

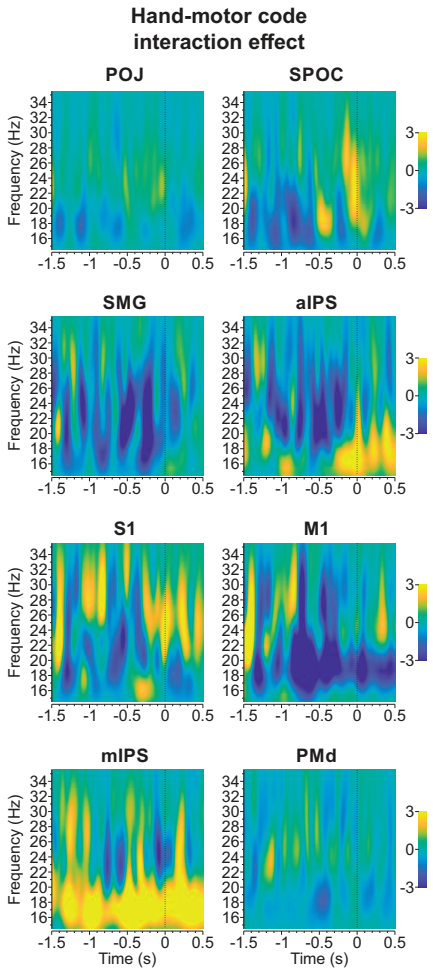

Figure 8. Lateralized hand-motor plan interaction effect analysis for beta-band activity. Same conventions as in Fig. 4 apply.

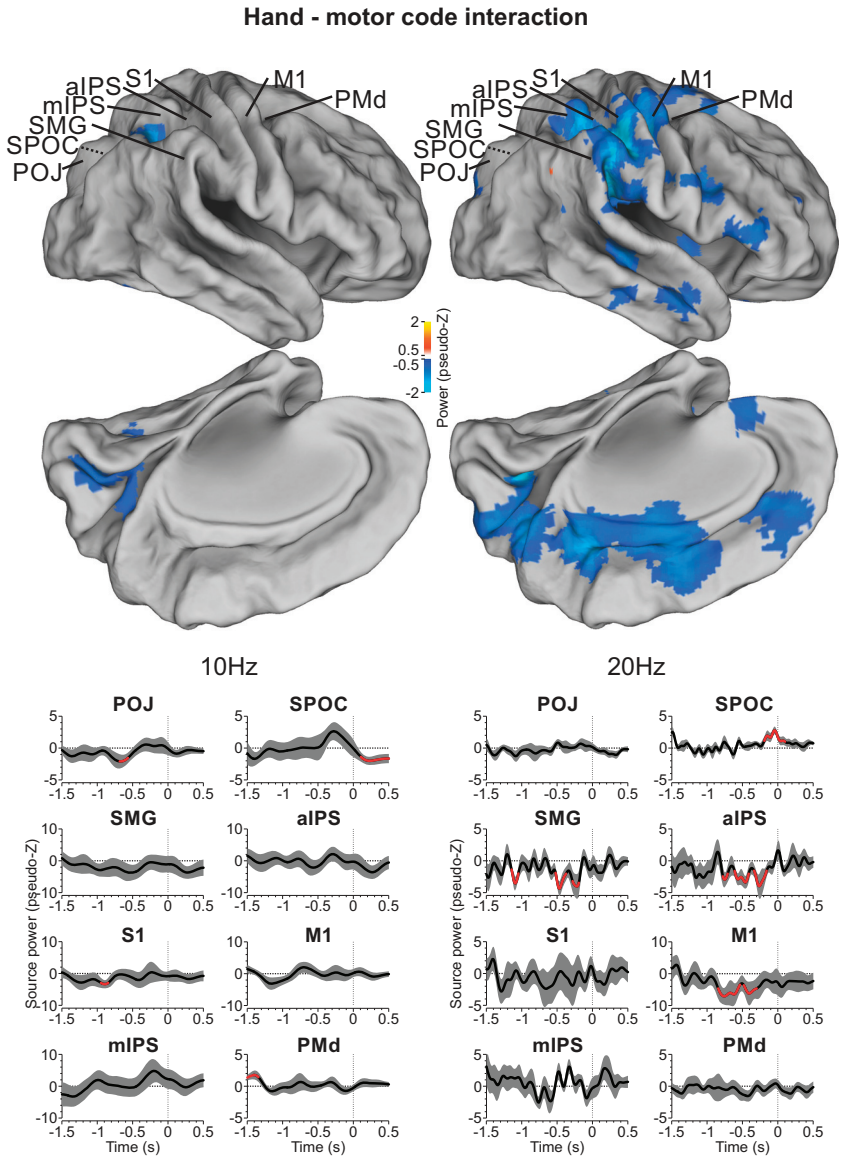

Figure 9. Hand specificity-motor coding interaction. Same conventions as Fig. 6 apply.

Summary: Location and Timing of Hand Specificity and Motor Integration

Figure 10 summarizes the results of both this and our previous study (42). Figure 10*A* shows the locations of the 16 bilateral sites that we studied, including 13 that showed instruction-dependent motor coding in our previous study (purple outer circles). Of those 13 motor coding areas, we report here 8 that also showed significant hand dependences (dark blue middle circles in Fig. 10*A*) and 6 that showed significant interactions between these two codes (cyan inner circles in Fig. 10*A*) in the present study. Both codes tended to be lateralized, with a consistent trend toward contralateral hand preference. It is noteworthy that, although the hand and motor plan networks largely overlapped, some areas (e.g., STS, AG, pIPS, SMA, PMv) only showed movement direction modulations, whereas others (mIPS, S1) only showed hand modulation. In general, motor coding was more broadly distributed, whereas lateralized hand position modulations were mostly clustered superior-medial in parietofrontal cortex (with the exception of SPOC). Importantly, a subset of the overlapping areas showed interactions between lateralized hand and motor planning modulations, signifying specific locations for hand-motor integration (aIPS, SMG, M1, SPOC).

Figure 10*B* shows the onset times of hand preference and hand-motor interactions relative to movement onset in the eight bilateral sites that showed significant hand modulation. Sites M1, mIPS, POJ, and S1 showed the earliest hand onsets, but of these only M1 showed an interaction with the motor plan. Sites PMd, aIPS, SPOC, and SMG show later onset but more interactions with the motor plan (in SPOC, aIPS and SMG). Figure 10*C* includes the timing of the top-down motor plan (derived from our pro/anti pointing instruction) and all 16 bilateral pairs. As reported previously (42), this plan seems to originate in (pre)frontal cortex but is only integrated with hand position in M1 and the more posterior sites described above. Importantly, we see early coding of both the top-down motor plan (in PMd, SMA, M1) and hand signals (M1, S1, POJ, mIPS) but their interactions occur

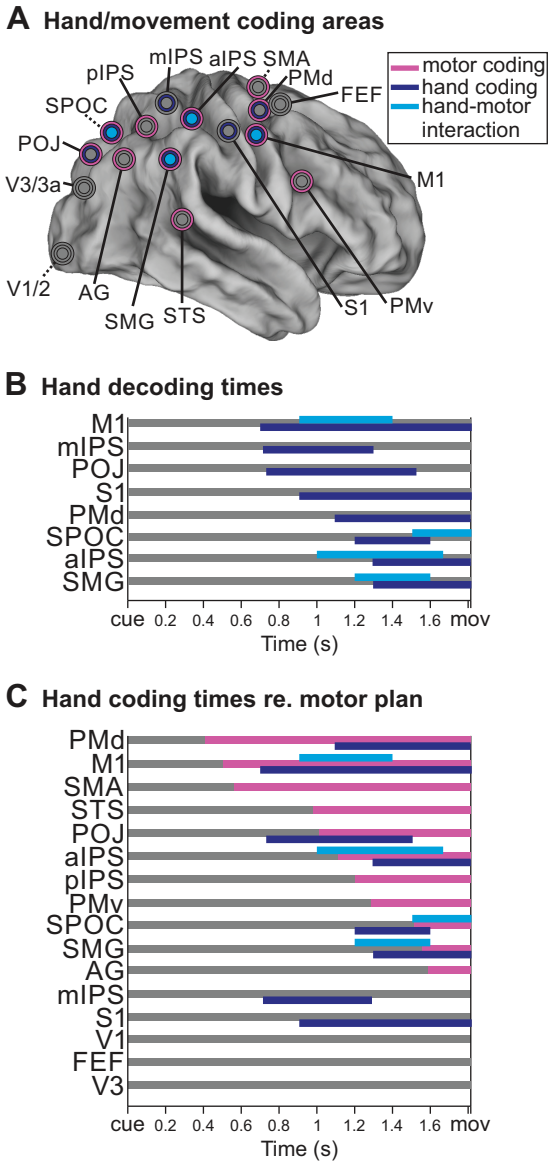

Figure 10. Summary of hand specificity and hand-motor code interaction effects. *A*: colors highlight sites showing significant motor coding (magenta), hand specificity (dark blue), and hand-motor code interactions (cyan). *B*: times when hand specificity (dark blue) and hand-motor code interactions (cyan) were significant. *C*: same times as in *B* overlaid with times of motor code significance (adapted from Ref. 42) for all 16 bilateral sites investigated and sorted by motor code onset time. AG, angular gyrus; aIPS, anterior interparietal sulcus; FEF, frontal eye fields; M1, primary motor cortex; mIPS, medial interparietal sulcus; pIPS, posterior interparietal sulcus; PMd, dorsal premotor cortex; PMv, ventral premotor cortex; POJ, parietooccipital junction; S1, primary somatosensory cortex; SMA, supplementary motor area; SMG, supramarginal gyrus; SPOC, superior parietooccipital cortex; STS, superior temporal sulcus.

later, in these and other (aIPS, SPOC, SMG) sites. This appears to suggest that hand selection and movement direction planning may initially arise independently, with later integration.

DISCUSSION

In this series of studies, we recorded MEG signals while human participants performed a pro/anti pointing task with left or right hand and then performed an ROI analysis on 16 bilateral cortical sites known to be involved in sensorimotor control. In our previous analysis, we only analyzed data from the right hand to identify instruction-dependent motor planning signals in 13 of these pairs (42). In the present analysis, we interrogated data for left versus right hand movements (pronation posture only) to ask two new and important questions: *1*) What is the extent, lateralization, and timing of hand-specific signals in the cerebral cortex? *2*) How, when, and where are these effector-specific signals integrated into the instruction-dependent motor command? Our analysis revealed that a subset of these areas differentially coded for which hand was used, including robust premotor activity in M1, S1, SMG, and aIPS with modest but still significant activation in POJ, SPOC, MIPS, and PMd. This hand main effect emerged gradually during the premotor period and, for some sites, prevailed across the movement (S1, M1, and PMd). Our next analysis found that only SPOC, SMG, aIPS, and M1 showed significant interactions of the effector with the movement plan, indicating a role in hand-motor integration (we did not find significant sensory hand-target direction interactions). As summarized in Fig. 10, hand and motor signals arose relatively early in the motor planning phase and, where they overlapped, only interacted later in the planning phase (close to motor execution).

Limitations and Caveats

Before considering the physiological implications of these findings, it is worth noting that, like any ROI analysis, our specific sites do not necessarily represent activity in the entire region they are named after, and their locations are best estimates given spatial resolution of the data (MRI/MEG), averaging, and source localization used here. Overall, a reasonable estimate is that these locations are accurate within ~5 mm, depending on local anatomy (44, 74). Given this, one may consider these ROI names and locations as guideposts rather than exactitudes. We consider more specific aspects of this when we compare our data to the literature below.

A related factor is the relative power and distortions of the MEG signal over gyri versus sulci. In theory, MEG is most sensitive to signals from the walls of sulci for which the cortical surface is orthogonal to the skull surface (77, 78). However, because of current spread, nonspherical skull surface, and few cortical surfaces being strictly parallel to the scalp, this is less of a concern in practice (45, 77–80). Another caveat is that subtraction methods assume linearity, whereas nonlinearities in the MEG signal could either exaggerate or compress differences in activation (62). Next, although MEG has practically unlimited temporal resolution, as in any such study temporal resolution is limited by synchronization with behavioral measures and averaging across participants. Finally, although the number of participants used in this study (performed >15 yr ago) is low by current standards, our key findings met current standards for power (see METHODS). This is likely because sensorimotor tasks yield high and consistent levels of brain activation relative to perception and cognition tasks (79) and because we had many trials for each participant (74). However, on the basis of these numbers, we cannot draw firm conclusions

from negative results. Given these caveats, our findings strongly support our hypotheses and generally agree with the neuroimaging and neurophysiological literature, as discussed below.

Instruction-Dependent Motor Codes

It is thought that frontal cortex plays an important role in instruction-dependent and nonstandard motor strategies, as opposed to reactive move-to-target strategies (81–83). For example, dorsolateral prefrontal cortex (DLPFC) is thought to be involved in response selection among multiple alternatives (84, 85). Both DLPFC and FEF are involved in preparatory set and task-switching in the oculomotor version of the pro/anti instruction task (38, 86, 87). Parietal cortex is also influenced by instructions for "nonstandard transformations" (36, 37), specifically causing reversals of motor tuning in primate parietal reach areas (40, 41). Even occipital cortex appears to be influenced by top-down motor signals from frontal cortex, although those early modulations are thought to involve imagery, attention, gating of sensory inputs, and/or compensation for expected sensory reafference (88–90).

In a previous functional (f)MRI study, we provided participants with a pro/anti reach instruction following a memory delay and then used contrasts similar to those used here to isolate visual versus motor directional tuning (14). Consistent with the discussion above, we found instruction-dependent modulations of directional tuning throughout occipital-parietal-frontal cortex, with major functional connectivity "hubs" in superior occipital gyrus (SOG), mIPS, AG, and SPOC, but were unable to determine temporal order. In our subsequent MEG study (42) we provided participants with the pro/anti instruction simultaneously with target appearance and performed a similar directional analysis on the resulting data. As shown here in Fig. 10*C* (magenta lines), this resulted in a sequence of motor recruitment proceeding from frontal toward parietal cortex. These same areas were selected for analysis here, and the motor vector contrast from that study was used for the hand-motor interaction analysis discussed below.

Left vs. Right Hand Coding

There is evidence for both effector-independent coding (7, 8, 10–12) and hand specificity throughout the parietofrontal reach system. Even primary motor cortex shows some signals related to the ipsilateral hand (9). Human neuroimaging studies show that parietofrontal cortex is bilaterally activated by unilateral reaches, but with a preference for the contralateral limb (6, 13–17, 19–21). Likewise, the monkey "parietal reach region," which spans the medial intraparietal sulcus and area V6A and probably corresponds to mIPS/SPOC (91), shows some ipsilateral signals (7, 92, 93) but is primarily modulated by reaches of the contralateral limb (7, 92).

In the present study, participants performed blocks of trials with either the left or right hand (and the other hand at rest) and so would need to attend to that hand for both sensory purposes, i.e., proprioceptive information about its location (27, 94, 118) and motor purposes, i.e., to gate motor commands for that hand (23, 95). Contrasting left and right hand pointing, we found robust premotor specificity in M1, S1, SMG, and aIPS, with modest but still significant activation in POJ, SPOC, mIPS, and PMd. Most of these are well known components of the reach system (35, 88). Inferior parietal cortex (specifically SMG) is an additional area of interest because it was also activated in our previous fMRI study (14), is involved in integrating visuospatial signals for grasp (48), and shows anatomic connectivity with temporal, prefrontal, and superior parietal cortex (96). In addition to SMG, V6A (likely corresponding to mIPS/SPOC; see above) is also involved in integrating visuospatial signals for grasping (97, 98), receives monosynaptic input from frontal and prefrontal areas (92), and might have a human homolog (99). aIPS neurons in monkeys (area AIP) are also tuned to left versus right hand use in grasping tasks (100).

Hand-Specific Movement Planning

As noted above, hand-specific information must be integrated into the motor plan, both to account for the correct location and to generate motor activation in the correct limb. Functional MRI studies of feedforward hand-target interactions suggest that target and hand-specific information may be integrated as early as parietal cortex, specifically in areas such as mid-posterior intraparietal sulcus (pIPS) (24, 28, 34), although effector-independent signals also may persist within frontal cortex (12). Brain stimulation studies have suggested that hand specificity first arises between SPOC and pIPS/AG, the posterior portion of inferior parietal cortex (52). Likewise, electrophysiological studies in monkeys show a progression of hand modulations on visual target signals at the single-unit level through parietal and frontal cortex (7, 30, 31, 33). We did not find significant hand-target interactions in the present task, perhaps because participants waited to process the pro/anti instruction before developing a movement plan, but cannot dismiss the possibility that these interactions still occurred at a subsignificant level undetectable in our analysis.

Much less is known about the integration of hand-specific signals into top-down motor plans. One potential difference here is there may already be hand specificity in top-down signals from motor and premotor areas (101). Some of our areas (SMA, STS, PMv, pIPS, AG) showed movement specificity but not a hand preference. Others (POJ, S1, mIPS, PMd) also code for hand selectivity but did not show an interaction with the motor code. Hand-motor plan interactions only occurred in a subset of areas: SPOC, SMG, aIPS, and M1. Hand-target interactions have been reported in monkeys (91), but these results seem to be at odds with human literature suggesting hand-target interactions in AG and mIPS (52). These differences might be accounted for by the task instruction (i.e., top-down vs. bottom-up), specific ROI coordinates (AG is quite large), and/or methodological and spatial resolution differences [MEG vs. fMRI and transcranial magnetic stimulation (TMS)].

It is noteworthy that our technique only detects extrinsic movement direction (i.e., left vs. right wrist rotation of either the left or right hand). However, the same extrinsic direction of wrist rotation requires opposite (radial/ulnar) deviations in opposite hands. Thus, once this becomes hand specific, one can deduce which muscles were likely involved. Based on our EMG recordings, this would require specific intrinsic synergies of activation in the extensor carpi radialis longus, extensor communis digitorum, extensor carpi ulnaris, and supinator longus (SL) muscles, as well as other forearm

muscles that we did not record from. This switch from extrinsic to intrinsic muscle coding is thought to only begin at the level of M1 (73). This could signify that our interaction results in M1 were related to this extrinsic-intrinsic conversion, whereas SPOC, SMG, and aIPS are likely related to higher-level aspects of hand-motor integration. For example, in our task we chose the hand for our participants, but in real-world circumstances these areas might be involved in hand choice for specific tasks (5).

Timing

Thus far we have discussed the spatial distribution of signals in our regions of interest. For this purpose, MEG has a lower spatial resolution than fMRI, but an important advantage of MEG is its higher temporal resolution. The relative activation of various signals in our regions of interest (summarized in Fig. 10) provides clues to the order of processing in our task. For example, it could be that in the anti reach task the brain waits until the final motor stage to "flip" the desired reach vector. Alternatively, frontal cortex could flip a high-level goal (opposite the stimulus) and then feed this back to hand-specific areas to recalculate the desired motor vector (14, 41, 43).

The timing of events in our data appears to be consistent with the latter possibility. First, besides visual signals (not shown here) one of the earliest signals that we observed was the instruction-dependent motor signal in frontal cortex, which then appears to feed back recurrently to parietal cortex. The next signal to emerge was hand specificity, suggesting a role in motor preparation. Notably, both these signals (hand and motor) were sustained through the action phase, suggesting that they play roles in both planning and execution (9). In contrast, the hand-motor interaction occurred closer to movement onset, suggesting a more specific role in planning (such as calculation of the motor vector). Overall, these results are consistent with the notion that the pro/anti instruction does not just influence the final motor output vector but causes updating and integration of hand-motor signals throughout parietofrontal cortex.

An interesting aspect of the timing of hand-specific motor commands (interaction effects) is that they first show up in M1. After M1, hand-specific motor commands later also appear in more posterior (parietal) areas. This succession of timing in the coding of the motor plan aligns with our previous finding (42) that sensory signals first undergo a feedforward transformation along the posterior-anterior axis, with motor coding first appearing in M1 and then gradually appearing in more posterior areas again. We have suggested that M1 updates the motor intention in more posterior regions once it has been computed after the initial feedforward transformation. Here, we show that early hand coding in M1 also leads to an early interaction effect. This hand-specific motor code then gradually appears in more posterior areas (SPOC, aIPS, SMG). Overall, this timing suggests that M1 is the main driver in establishing a hand-specific motor code.

Frequency Specificity

Another advantage of MEG is its capacity to isolate frequency-specific effects (102). This is interesting because different frequencies are associated with different processes in the brain, e.g., alpha-band modulations indicate sensory processing (103–106) and beta-band modulations accompany motor planning and control (79, 103, 107–113). Consistent with sensory coding of hand use, we found a main hand effect in alpha band. We also found a main hand effect in beta band, which makes sense given that this was a movement planning task. At the same time, we only observed a significant interaction effect in the beta band, suggesting that this interaction effect reflects the actual motor plan specific to the hand used. At the same time, our previous study (42) showed that an abstract (not hand specific) motor intention was decodable from both alpha and beta bands. Although we cannot interpret negative results (i.e., absence of alpha interaction effects), our results are certainly consistent with a sensory-to-motor transformation using sensory hand and target information and transforming it into a hand-specific motor plan.

Correlation vs. Causality

The ultimate challenge for this area of research is to reconcile the evidence for hand preference for bilateral hand representation in the reach system, even down to the level of primary motor cortex (9, 114, 115). An important distinction here is between correlation and causality: techniques such as unit recording, fMRI, and MEG show the presence of signals but do not necessarily imply a causal relation to the movement. A growing consensus is that, despite bilateral representation, contralateral causality emerges as early as the parietal reach region (23, 95). Ipsilateral signals might play other roles such as bilateral coordination (116, 117) but could be filtered out for contralateral control through parcellation of signals (9, 114, 115).

Conclusions

Together with our previous study (42), these results demonstrate a specific whole brain topography for hand-specific signals and instruction-dependent motor signals in parietofrontal cortex, in both the alpha and beta bands. In contrast, hand-motor interactions primarily occurred in the beta bands and in a smaller subset of frontoparietal regions. The timing of these events suggests that in an instruction-dependent pro/anti pointing task, the motor strategy (same or opposite to visual stimulus) is determined in frontal cortex and then propagates backward to parietal cortex, with premotor hand-motor interactions occurring later before movement onset. Generalizing from these results, we suggest that top-down, instruction-dependent, and/or abstract motor strategies show a sequence and topography different from bottom-up hand-target interactions in the feedforward occipital-parietal-frontal path.

SUPPLEMENTAL MATERIALS

Supplemental Figs. S1 and S2: https://doi.org/10.6084/m9.figshare.19962224.

ACKNOWLEDGMENTS

The authors thank Andreea Bostan, William Gaetz, Herbert Goltz, and Sonja Bells for technical assistance during data collection.

GRANTS

Experiments were supported by a Canadian Institutes for Health Research Grant held by J.D.C. G.B. was supported by a Marie Curie Fellowship (European Union) during the experiments and by the National Sciences and Engineering Research Council (NSERC) (Canada) thereafter. During these studies, J.D.C. was supported by a Canada Research Chair.

DISCLOSURES

No conflicts of interest, financial or otherwise, are declared by the authors.

AUTHOR CONTRIBUTIONS

G.B., D.O.C., and J.C. conceived and designed research; G.B. performed experiments; G.B. analyzed data; G.B., D.O.C., and J.C. interpreted results of experiments; G.B. prepared figures; G.B. and J.C. drafted manuscript; G.B., D.O.C., and J.C. edited and revised manuscript; G.B., D.O.C., and J.C. approved final version of manuscript.

REFERENCES

1. **Andersen RA**, **Cui H.** Intention, action planning, and decision making in parietal-frontal circuits. *Neuron* 63: 568–583, 2009. doi:10.1016/j.neuron.2009.08.028.
2. **Crawford JD**, **Henriques DY**, **Medendorp WP.** Three-dimensional transformations for goal-directed action. *Annu Rev Neurosci* 34: 309–331, 2011. doi:10.1146/annurev-neuro-061010-113749.
3. **Hadjidimitrakis K**, **Bertozzi F**, **Breveglieri R**, **Fattori P**, **Galletti C.** Body-centered, mixed, but not hand-centered coding of visual targets in the medial posterior parietal cortex during reaches in 3D space. *Cereb Cortex* 24: 3209–3220, 2014. doi:10.1093/cercor/bht181.
4. **Cisek P**, **Kalaska JF.** Neural mechanisms for interacting with a world full of action choices. *Annu Rev Neurosci* 33: 269–298, 2010. doi:10.1146/annurev.neuro.051508.135409.
5. **Scharoun SM**, **Scanlan KA**, **Bryden PJ.** Hand and grasp selection in a preferential reaching task: the effects of object location, orientation, and task intention. *Front Psychol* 7: 360, 2016. doi:10.3389/fpsyg.2016.00360.
6. **Filimon F**, **Nelson JD**, **Huang RS**, **Sereno MI.** Multiple parietal reach regions in humans: cortical representations for visual and proprioceptive feedback during on-line reaching. *J Neurosci* 29: 2961–2971, 2009. doi:10.1523/JNEUROSCI.3211-08.2009.
7. **Chang SW**, **Dickinson AR**, **Snyder LH.** Limb-specific representation for reaching in the posterior parietal cortex. *J Neurosci* 28: 6128–6140, 2008. doi:10.1523/JNEUROSCI.1442-08.2008.
8. **Donchin O**, **Gribova A**, **Steinberg O**, **Bergman H**, **Vaadia E.** Primary motor cortex is involved in bimanual coordination. *Nature* 395: 274–278, 1998. doi:10.1038/26220.
9. **Heming EA**, **Cross KP**, **Takei T**, **Cook DJ**, **Scott SH.** Independent representations of ipsilateral and contralateral limbs in primary motor cortex. *eLife* 8: e48190, 2019. doi:10.7554/eLife.48190.
10. **Matsunami K**, **Hamada I.** Characteristics of the ipsilateral movement-related neuron in the motor cortex of the monkey. *Brain Res* 204: 29–42, 1981. doi:10.1016/0006-8993(81)90649-1.
11. **Tanji J**, **Okano K**, **Sato KC.** Neuronal activity in cortical motor areas related to ipsilateral, contralateral, and bilateral digit movements of the monkey. *J Neurophysiol* 60: 325–343, 1988. doi:10.1152/jn.1988.60.1.325.
12. **Wiestler T**, **Waters-Metenier S**, **Diedrichsen J.** Effector-independent motor sequence representations exist in extrinsic and intrinsic reference frames. *J Neurosci* 34: 5054–5064, 2014. doi:10.1523/JNEUROSCI.5363-13.2014.
13. **Bernier PM**, **Grafton ST.** Human posterior parietal cortex flexibly determines reference frames for reaching based on sensory context. *Neuron* 68: 776–788, 2010. doi:10.1016/j.neuron.2010.11.002.
14. **Cappadocia DC**, **Monaco S**, **Chen Y**, **Blohm G**, **Crawford JD.** Temporal evolution of target representation, movement direction planning, and reach execution in occipital-parietal-frontal cortex: an fMRI study. *Cereb Cortex* 27: 5242–5260, 2017. doi:10.1093/cercor/bhw304.
15. **Cavina-Pratesi C**, **Monaco S**, **Fattori P**, **Galletti C**, **McAdam TD**, **Quinlan DJ**, **Goodale MA**, **Culham JC.** Functional magnetic resonance imaging reveals the neural substrates of arm transport and grip formation in reach-to-grasp actions in humans. *J Neurosci* 30: 10306–10323, 2010. doi:10.1523/JNEUROSCI.2023-10.2010.
16. **Connolly JD**, **Andersen RA**, **Goodale MA.** FMRI evidence for a "parietal reach region" in the human brain. *Exp Brain Res* 153: 140–145, 2003. doi:10.1007/s00221-003-1587-1.
17. **Gallivan JP**, **McLean DA**, **Smith FW**, **Culham JC.** Decoding effector-dependent and effector-independent movement intentions from human parieto-frontal brain activity. *J Neurosci* 31: 17149–17168, 2011. doi:10.1523/JNEUROSCI.1058-11.2011.
18. **Gallivan JP**, **McLean DA**, **Valyear KF**, **Pettypiece CE**, **Culham JC.** Decoding action intentions from preparatory brain activity in human parieto-frontal networks. *J Neurosci* 31: 9599–9610, 2011. doi:10.1523/JNEUROSCI.0080-11.2011.
19. **Gallivan JP**, **Wood DK.** Simultaneous encoding of potential grasping movements in macaque anterior intraparietal area. *J Neurosci* 29: 12031–12032, 2009. doi:10.1523/JNEUROSCI.3245-09.2009.
20. **Medendorp WP**, **Goltz HC**, **Vilis T**, **Crawford JD.** Gaze-centered updating of visual space in human parietal cortex. *J Neurosci* 23: 6209–6214, 2003. doi:10.1523/JNEUROSCI.23-15-06209.2003.
21. **Prado J**, **Clavagnier S**, **Otzenberger H**, **Scheiber C**, **Kennedy H**, **Perenin MT.** Two cortical systems for reaching in central and peripheral vision. *Neuron* 48: 849–858, 2005. doi:10.1016/j.neuron.2005.10.010.
22. **Mooshagian E**, **Wang C**, **Holmes CD**, **Snyder LH.** Single units in the posterior parietal cortex encode patterns of bimanual coordination. *Cereb Cortex* 28: 1549–1567, 2018. doi:10.1093/cercor/bhx052.
23. **Mooshagian E**, **Yttri EA**, **Loewy AD**, **Snyder LH.** Contralateral limb specificity for movement preparation in the parietal reach region. *J Neurosci* 42: 1692–1701, 2022. doi:10.1523/JNEUROSCI.0232-21.2021.
24. **Gallivan JP**, **McLean DA**, **Flanagan JR**, **Culham JC.** Where one hand meets the other: limb-specific and action-dependent movement plans decoded from preparatory signals in single human frontoparietal brain areas. *J Neurosci* 33: 1991–2008, 2013. doi:10.1523/JNEUROSCI.0541-12.2013.
25. **Ting LH**, **McKay JL.** Neuromechanics of muscle synergies for posture and movement. *Curr Opin Neurobiol* 17: 622–628, 2007. doi:10.1016/j.conb.2008.01.002.
26. **Khan AZ**, **Crawford JD**, **Blohm G**, **Urquizar C**, **Rossetti Y**, **Pisella L.** Influence of initial hand and target position on reach errors in optic ataxic and normal subjects. *J Vis* 7: 8.1–8.16, 2007. doi:10.1167/7.5.8.
27. **Sober SJ**, **Sabes PN.** Multisensory integration during motor planning. *J Neurosci* 23: 6982–6992, 2003. doi:10.1523/JNEUROSCI.23-18-06982.2003.
28. **Beurze SM**, **de Lange FP**, **Toni I**, **Medendorp WP.** Integration of target and effector information in the human brain during reach planning. *J Neurophysiol* 97: 188–199, 2007. doi:10.1152/jn.00456.2006.
29. **Buneo CA**, **Andersen RA.** The posterior parietal cortex: sensorimotor interface for the planning and online control of visually guided movements. *Neuropsychologia* 44: 2594–2606, 2006. doi:10.1016/j.neuropsychologia.2005.10.011.
30. **Chang SW**, **Snyder LH.** The representations of reach endpoints in posterior parietal cortex depend on which hand does the reaching. *J Neurophysiol* 107: 2352–2365, 2012. doi:10.1152/jn.00852.2011.
31. **Cisek P**, **Crammond DJ**, **Kalaska JF.** Neural activity in primary motor and dorsal premotor cortex in reaching tasks with the contralateral versus ipsilateral arm. *J Neurophysiol* 89: 922–942, 2003. doi:10.1152/jn.00607.2002.
32. **Fattori P**, **Breveglieri R**, **Raos V**, **Bosco A**, **Galletti C.** Vision for action in the macaque medial posterior parietal cortex. *J Neurosci* 32: 3221–3234, 2012. doi:10.1523/JNEUROSCI.5358-11.2012.
33. **Hoshi E**, **Tanji J.** Integration of target and body-part information in the premotor cortex when planning action. *Nature* 408: 466–470, 2000. doi:10.1038/35044075.
34. **Medendorp WP**, **Goltz HC**, **Crawford JD**, **Vilis T.** Integration of target and effector information in human posterior parietal cortex for the planning of action. *J Neurophysiol* 93: 954–962, 2005. doi:10.1152/jn.00725.2004.

35. **Vesia M**, **Crawford JD.** Specialization of reach function in human posterior parietal cortex. *Exp Brain Res* 221: 1–18, 2012. doi:10.1007/s00221-012-3158-9.
36. **Hawkins KM**, **Sergio LE.** Visuomotor impairments in older adults at increased Alzheimer's disease risk. *J Alzheimers Dis* 42: 607–621, 2014. doi:10.3233/JAD-140051.
37. **Sayegh PF**, **Gorbet DJ**, **Hawkins KM**, **Hoffman KL**, **Sergio LE.** the contribution of different cortical regions to the control of spatially decoupled eye-hand coordination. *J Cogn Neurosci* 29: 1194–1211, 2017. doi:10.1162/jocn_a_01111.
38. **Connolly JD**, **Goodale MA**, **DeSouza JF**, **Menon RS**, **Vilis T.** A comparison of frontoparietal fMRI activation during anti-saccades and anti-pointing. *J Neurophysiol* 84: 1645–1655, 2000. doi:10.1152/jn.2000.84.3.1645.
39. **Gail A**, **Andersen RA.** Neural dynamics in monkey parietal reach region reflect context-specific sensorimotor transformations. *J Neurosci* 26: 9376–9384, 2006. doi:10.1523/JNEUROSCI.1570-06.2006.
40. **Gail A**, **Klaes C**, **Westendorff S.** Implementation of spatial transformation rules for goal-directed reaching via gain modulation in monkey parietal and premotor cortex. *J Neurosci* 29: 9490–9499, 2009. doi:10.1523/JNEUROSCI.1095-09.2009.
41. **Kuang S**, **Morel P**, **Gail A.** Planning movements in visual and physical space in monkey posterior parietal cortex. *Cereb Cortex* 26: 731–747, 2016. doi:10.1093/cercor/bhu312.
42. **Blohm G**, **Alikhanian H**, **Gaetz W**, **Goltz HC**, **DeSouza JF**, **Cheyne DO**, **Crawford JD.** Neuromagnetic signatures of the spatiotemporal transformation for manual pointing. *NeuroImage* 197: 306–319, 2019. doi:10.1016/j.neuroimage.2019.04.074.
43. **Fernandez-Ruiz J**, **Goltz HC**, **DeSouza JF**, **Vilis T**, **Crawford JD.** Human parietal "reach region" primarily encodes intrinsic visual direction, not extrinsic movement direction, in a visual motor dissociation task. *Cereb Cortex* 17: 2283–2292, 2007. doi:10.1093/cercor/bhl137.
44. **Alikhanian H**, **Crawford JD**, **DeSouza JF**, **Cheyne DO**, **Blohm G.** Adaptive cluster analysis approach for functional localization using magnetoencephalography. *Front Neurosci* 7: 73, 2013. doi:10.3389/fnins.2013.00073.
45. **Baillet S.** Magnetoencephalography for brain electrophysiology and imaging. *Nat Neurosci* 20: 327–339, 2017. doi:10.1038/nn.4504.
46. **Niso G**, **Krol LR**, **Combrisson E**, **Dubarry AS**, **Elliott MA**, **François C**, **Héjja-Brichard Y**, **Herbst SK**, **Jerbi K**, **Kovic V**, **Lehongre K**, **Luck SJ**, **Mercier M**, **Mosher JC**, **Pavlov YG**, **Puce A**, **Schettino A**, **Schön D**, **Sinnott-Armstrong W**, **Somon B**, **Šoškić A**, **Styles SJ**, **Tibon R**, **Vilas MG**, **van Vliet M**, **Chaumon M.** Good scientific practice in MEEG research: progress and perspectives. *NeuroImage* 257: 119056, 2022. doi:10.1016/j.neuroimage.2022.119056.
47. **Shattuck DW**, **Leahy RM.** BrainSuite: an automated cortical surface identification tool. *Med Image Anal* 6: 129–142, 2002. doi:10.1016/s1361-8415(02)00054-3.
48. **Baltaretu BR**, **Monaco S**, **Velji-Ibrahim J**, **Luabeya GN**, **Crawford JD.** Parietal cortex integrates saccade and object orientation signals to update grasp plans. *J Neurosci* 40: 4525–4535, 2020. doi:10.1523/JNEUROSCI.0300-20.2020.
49. **Cappadocia DC**, **Monaco S**, **Chen Y**, **Crawford JD.** Cortical mechanisms for reaches versus saccades: progression of effector-specificity through target memory to movement planning and execution (Preprint). *bioRxiv* 415562, 2018. doi:10.1101/415562.
50. **Martínez A**, **Di Russo F**, **Anllo-Vento L**, **Sereno MI**, **Buxton RB**, **Hillyard SA.** Putting spatial attention on the map: timing and localization of stimulus selection processes in striate and extrastriate visual areas. *Vision Res* 41: 1437–1457, 2001. doi:10.1016/S0042-6989(00)00267-4.
51. **Tootell RB**, **Mendola JD**, **Hadjikhani NK**, **Ledden PJ**, **Liu AK**, **Reppas JB**, **Sereno MI**, **Dale AM.** Functional analysis of V3A and related areas in human visual cortex. *J Neurosci* 17: 7060–7078, 1997. doi:10.1523/JNEUROSCI.17-18-07060.1997.
52. **Vesia M**, **Prime SL**, **Yan X**, **Sergio LE**, **Crawford JD.** Specificity of human parietal saccade and reach regions during transcranial magnetic stimulation. *J Neurosci* 30: 13053–13065, 2010. doi:10.1523/JNEUROSCI.1644-10.2010.
53. **Bremmer F**, **Schlack A**, **Duhamel JR**, **Graf W**, **Fink GR.** Space coding in primate posterior parietal cortex. *NeuroImage* 14: S46–S51, 2001. doi:10.1006/nimg.2001.0817.
54. **Blangero A**, **Menz MM**, **McNamara A**, **Binkofski F.** Parietal modules for reaching. *Neuropsychologia* 47: 1500–1507, 2009. doi:10.1016/j.neuropsychologia.2008.11.030.
55. **Nickel J**, **Seitz RJ.** Functional clusters in the human parietal cortex as revealed by an observer-independent meta-analysis of functional activation studies. *Anat Embryol (Berl)* 210: 463–472, 2005. doi:10.1007/s00429-005-0037-1.
56. **Grosbras MH**, **Laird AR**, **Paus T.** Cortical regions involved in eye movements, shifts of attention, and gaze perception. *Hum Brain Mapp* 25: 140–154, 2005. doi:10.1002/hbm.20145.
57. **Mayka MA**, **Corcos DM**, **Leurgans SE**, **Vaillancourt DE.** Three-dimensional locations and boundaries of motor and premotor cortices as defined by functional brain imaging: a meta-analysis. *NeuroImage* 31: 1453–1474, 2006. doi:10.1016/j.neuroimage.2006.02.004.
58. **Connolly JD**, **Goodale MA**, **Cant JS**, **Munoz DP.** Effector-specific fields for motor preparation in the human frontal cortex. *NeuroImage* 34: 1209–1219, 2007. doi:10.1016/j.neuroimage.2006.10.001.
59. **Paus T.** Location and function of the human frontal eye-field: a selective review. *Neuropsychologia* 34: 475–483, 1996. doi:10.1016/0028-3932(95)00134-4.
60. **Cheyne D**, **Bells S**, **Ferrari P**, **Gaetz W**, **Bostan AC.** Self-paced movements induce high-frequency gamma oscillations in primary motor cortex. *NeuroImage* 42: 332–342, 2008. doi:10.1016/j.neuroimage.2008.04.178.
61. **Cheyne D**, **Bostan AC**, **Gaetz W**, **Pang EW.** Event-related beamforming: a robust method for presurgical functional mapping using MEG. *Clin Neurophysiol* 118: 1691–1704, 2007. doi:10.1016/j.clinph.2007.05.064.
62. **Hadjipapas A**, **Hillebrand A**, **Holliday IE**, **Singh KD**, **Barnes GR.** Assessing interactions of linear and nonlinear neuronal sources using MEG beamformers: a proof of concept. *Clin Neurophysiol* 116: 1300–1313, 2005. doi:10.1016/j.clinph.2005.01.014.
63. **Vrba J**, **Robinson SE.** Signal processing in magnetoencephalography. *Methods* 25: 249–271, 2001. doi:10.1006/meth.2001.1238.
64. **Jobst C**, **Ferrari P**, **Isabella S**, **Cheyne D.** BrainWave: A Matlab toolbox for beamformer source analysis of MEG data. *Front Neurosci* 12: 587, 2018. doi:10.3389/fnins.2018.00587.
65. **Neugebauer F**, **Möddel G**, **Rampp S**, **Burger M**, **Wolters CH.** The effect of head model simplification on beamformer source localization. *Front Neurosci* 11: 625, 2017. doi:10.3389/fnins.2017.00625.
66. **Sekihara K**, **Sahani M**, **Nagarajan SS.** Localization bias and spatial resolution of adaptive and non-adaptive spatial filters for MEG source reconstruction. *NeuroImage* 25: 1056–1067, 2005. doi:10.1016/j.neuroimage.2004.11.051.
67. **Kilner JM.** Bias in a common EEG and MEG statistical analysis and how to avoid it. *Clin Neurophysiol* 124: 2062–2063, 2013. doi:10.1016/j.clinph.2013.03.024.
68. **Kriegeskorte N**, **Simmons WK**, **Bellgowan PS**, **Baker CI.** Circular analysis in systems neuroscience: the dangers of double dipping. *Nat Neurosci* 12: 535–540, 2009. doi:10.1038/nn.2303.
69. **Van Essen DC.** A population-average, landmark- and surface-based (PALS) atlas of human cerebral cortex. *NeuroImage* 28: 635–662, 2005. doi:10.1016/j.neuroimage.2005.06.058.
70. **Van Essen DC**, **Drury HA**, **Dickson J**, **Harwell J**, **Hanlon D**, **Anderson CH.** An integrated software suite for surface-based analyses of cerebral cortex. *J Am Med Inform Assoc* 8: 443–459, 2001. doi:10.1136/jamia.2001.0080443.
71. **Van Der Werf J**, **Jensen O**, **Fries P**, **Medendorp WP.** Gamma-band activity in human posterior parietal cortex encodes the motor goal during delayed prosaccades and antisaccades. *J Neurosci* 28: 8397–8405, 2008. doi:10.1523/JNEUROSCI.0630-08.2008.
72. **Gertz H**, **Fiehler K.** Human posterior parietal cortex encodes the movement goal in a pro-/anti-reach task. *J Neurophysiol* 114: 170–183, 2015. doi:10.1152/jn.01039.2014.
73. **Kakei S**, **Hoffman DS**, **Strick PL.** Direction of action is represented in the ventral premotor cortex. *Nat Neurosci* 4: 1020–1025, 2001. doi:10.1038/nn726.
74. **Chaumon M**, **Puce A**, **George N.** Statistical power: implications for planning MEG studies. *NeuroImage* 233: 117894, 2021. doi:10.1016/j.neuroimage.2021.117894.
75. **Maris E**, **Oostenveld R.** Nonparametric statistical testing of EEG- and MEG-data. *J Neurosci Methods* 164: 177–190, 2007. doi:10.1016/j.jneumeth.2007.03.024.

76. **Pfurtscheller G**, **Lopes da Silva FH.** Event-related EEG/MEG synchronization and desynchronization: basic principles. *Clin Neurophysiol* 110: 1842–1857, 1999. doi:10.1016/S1388-2457(99)00141-8.
77. **Goldenholz DM**, **Ahlfors SP**, **Hämäläinen MS**, **Sharon D**, **Ishitobi M**, **Vaina LM**, **Stufflebeam SM.** Mapping the signal-to-noise-ratios of cortical sources in magnetoencephalography and electroencephalography. *Hum Brain Mapp* 30: 1077–1086, 2009. doi:10.1002/hbm.20571.
78. **Hillebrand A**, **Barnes GR.** A quantitative assessment of the sensitivity of whole-head MEG to activity in the adult human cortex. *NeuroImage* 16: 638–650, 2002. doi:10.1006/nimg.2002.1102.
79. **Cheyne DO.** MEG studies of sensorimotor rhythms: a review. *Exp Neurol* 245: 27–39, 2013. doi:10.1016/j.expneurol.2012.08.030.
80. **Koser K.** Introduction: international migration and global governance. *Glob Gov* 16: 301–315, 2010. doi:10.1163/19426720-01603001.
81. **Bonnard M**, **de Graaf J**, **Pailhous J.** Interactions between cognitive and sensorimotor functions in the motor cortex: evidence from the preparatory motor sets anticipating a perturbation. *Rev Neurosci* 15: 371–382, 2004. doi:10.1515/revneuro.2004.15.5.371.
82. **Coe BC**, **Munoz DP.** Mechanisms of saccade suppression revealed in the anti-saccade task. *Philos Trans R Soc Lond B, Biol Sci* 372: 20160192, 2017. doi:10.1098/rstb.2016.0192.
83. **Hwang EJ**, **Sato TR**, **Sato TK.** A canonical scheme of bottom-up and top-down information flows in the frontoparietal network. *Front Neural Circuits* 15: 691314, 2021. doi:10.3389/fncir.2021.691314.
84. **Rowe JB**, **Toni I**, **Josephs O**, **Frackowiak RS**, **Passingham RE.** The prefrontal cortex: response selection or maintenance within working memory? *Science* 288: 1656–1660, 2000. doi:10.1126/science.288.5471.1656.
85. **van Eimeren T**, **Wolbers T**, **Münchau A**, **Büchel C**, **Weiller C**, **Siebner HR.** Implementation of visuospatial cues in response selection. *NeuroImage* 29: 286–294, 2006. doi:10.1016/j.neuroimage.2005.07.014.
86. **Connolly JD**, **Goodale MA**, **Menon RS**, **Munoz DP.** Human fMRI evidence for the neural correlates of preparatory set. *Nat Neurosci* 5: 1345–1352, 2002. doi:10.1038/nn969.
87. **DeSouza JF**, **Menon RS**, **Everling S.** Preparatory set associated with pro-saccades and anti-saccades in humans investigated with event-related fMRI. *J Neurophysiol* 89: 1016–1023, 2003. doi:10.1152/jn.00562.2002.
88. **Gallivan JP**, **Culham JC.** Neural coding within human brain areas involved in actions. *Curr Opin Neurobiol* 33: 141–149, 2015. doi:10.1016/j.conb.2015.03.012.
89. **Monaco S**, **Malfatti G**, **Culham JC**, **Cattaneo L**, **Turella L.** Decoding motor imagery and action planning in the early visual cortex: overlapping but distinct neural mechanisms. *NeuroImage* 218: 116981, 2020. doi:10.1016/j.neuroimage.2020.116981.
90. **Moore T**, **Zirnsak M.** Neural mechanisms of selective visual attention. *Annu Rev Psychol* 68: 47–72, 2017. doi:10.1146/annurev-psych-122414-033400.
91. **Passarelli L**, **Gamberini M**, **Fattori P.** The superior parietal lobule of primates: a sensory-motor hub for interaction with the environment. *J Integr Neurosci* 20: 157–171, 2021. doi:10.31083/j.jin.2021.01.334.
92. **Gamberini M**, **Passarelli L**, **Fattori P**, **Galletti C.** Structural connectivity and functional properties of the macaque superior parietal lobule. *Brain Struct Funct* 225: 1349–1367, 2020. doi:10.1007/s00429-019-01976-9.
93. **Merrick CM**, **Dixon TC**, **Breska A**, **Lin J**, **Chang EF**, **King-Stephens D**, **Laxer KD**, **Weber PB**, **Carmena J**, **Thomas Knight R**, **Ivry RB.** Left hemisphere dominance for bilateral kinematic encoding in the human brain. *eLife* 11: e69977, 2022. doi:10.7554/eLife.69977.
94. **Burns JK**, **Blohm G.** Multi-sensory weights depend on contextual noise in reference frame transformations. *Front Hum Neurosci* 4: 221, 2010. doi:10.3389/fnhum.2010.00221.
95. **Yttri EA**, **Wang C**, **Liu Y**, **Snyder LH.** The parietal reach region is limb specific and not involved in eye-hand coordination. *J Neurophysiol* 111: 520–532, 2014. doi:10.1152/jn.00058.2013.
96. **Vickery S**, **Eickhoff SB**, **Friedrich P.** Hemispheric specialization of the primate inferior parietal lobule. *Neurosci Bull* 38: 334–336, 2022. doi:10.1007/s12264-021-00807-4.
97. **Fattori P**, **Breveglieri R**, **Bosco A**, **Gamberini M**, **Galletti C.** Vision for prehension in the medial parietal cortex. *Cereb Cortex* 27: 1149–1163, 2017. doi:10.1093/cercor/bhv302.
98. **Galletti C**, **Fattori P.** The dorsal visual stream revisited: stable circuits or dynamic pathways? *Cortex* 98: 203–217, 2018. doi:10.1016/j.cortex.2017.01.009.
99. **Tosoni A**, **Pitzalis S**, **Committeri G**, **Fattori P**, **Galletti C**, **Galati G.** Resting-state connectivity and functional specialization in human medial parieto-occipital cortex. *Brain Struct Funct* 220: 3307–3321, 2015. doi:10.1007/s00429-014-0858-x.
100. **Michaels JA**, **Scherberger H.** Population coding of grasp and laterality-related information in the macaque fronto-parietal network. *Sci Rep* 8: 1710, 2018. doi:10.1038/s41598-018-20051-7.
101. **Scott SH.** A functional taxonomy of bottom-up sensory feedback processing for motor actions. *Trends Neurosci* 39: 512–526, 2016. doi:10.1016/j.tins.2016.06.001.
102. **Cabral J**, **Castaldo F**, **Vohryzek J**, **Litvak V**, **Bick C**, **Lambiotte R**, **Friston K**, **Kringelbach ML**, **Deco G.** Metastable oscillatory modes emerge from synchronization in the brain spacetime connectome. *Commun Phys* 5: 1–13, 2022. doi:10.1038/s42005-021-00784-0.
103. **Buchholz VN**, **Jensen O**, **Medendorp WP.** Different roles of alpha and beta band oscillations in anticipatory sensorimotor gating. *Front Hum Neurosci* 8: 446, 2014. doi:10.3389/fnhum.2014.00446.
104. **Jensen O**, **Gelfand J**, **Kounios J**, **Lisman JE.** Oscillations in the alpha band (9-12 Hz) increase with memory load during retention in a short-term memory task. *Cereb Cortex* 12: 877–882, 2002. doi:10.1093/cercor/12.8.877.
105. **Klimesch W.** α-Band oscillations, attention, and controlled access to stored information. *Trends Cogn Sci* 16: 606–617, 2012. doi:10.1016/j.tics.2012.10.007.
106. **Palva S**, **Palva JM.** New vistas for alpha-frequency band oscillations. *Trends Neurosci* 30: 150–158, 2007. doi:10.1016/j.tins.2007.02.001.
107. **Isabella S**, **Ferrari P**, **Jobst C**, **Cheyne JA**, **Cheyne D.** Complementary roles of cortical oscillations in automatic and controlled processing during rapid serial tasks. *NeuroImage* 118: 268–281, 2015. doi:10.1016/j.neuroimage.2015.05.081.
108. **Kilavik BE**, **Zaepffel M**, **Brovelli A**, **MacKay WA**, **Riehle A.** The ups and downs of β oscillations in sensorimotor cortex. *Exp Neurol* 245: 15–26, 2013. doi:10.1016/j.expneurol.2012.09.014.
109. **Lopes da Silva F.** EEG and MEG: relevance to neuroscience. *Neuron* 80: 1112–1128, 2013. doi:10.1016/j.neuron.2013.10.017.
110. **Neuper C**, **Pfurtscheller G.** Evidence for distinct beta resonance frequencies in human EEG related to specific sensorimotor cortical areas. *Clin Neurophysiol* 112: 2084–2097, 2001. doi:10.1016/S1388-2457(01)00661-7.
111. **Neuper C**, **Wörtz M**, **Pfurtscheller G.** ERD/ERS patterns reflecting sensorimotor activation and deactivation. *Prog Brain Res* 159: 211–222, 2006. doi:10.1016/S0079-6123(06)59014-4.
112. **Spitzer B**, **Haegens S.** Beyond the status quo: a role for beta oscillations in endogenous content (re)activation. *eNeuro* 4: ENEURO.0170-17.2017, 2017. doi:10.1523/ENEURO.0170-17.2017.
113. **Van Der Werf J**, **Buchholz VN**, **Jensen O**, **Medendorp WP.** Neuronal synchronization in human parietal cortex during saccade planning. *Behav Brain Res* 205: 329–335, 2009. doi:10.1016/j.bbr.2009.06.011.
114. **Ames KC**, **Churchland MM.** Motor cortex signals for each arm are mixed across hemispheres and neurons yet partitioned within the population response. *eLife* 8: e46159, 2019. doi:10.7554/eLife.46159.
115. **Bundy DT**, **Leuthardt EC.** The cortical physiology of ipsilateral limb movements. *Trends Neurosci* 42: 825–839, 2019. doi:10.1016/j.tins.2019.08.008.
116. **Le A**, **Niemeier M.** Visual field preferences of object analysis for grasping with one hand. *Front Hum Neurosci* 8: 782, 2014. doi:10.3389/fnhum.2014.00782.
117. **Le A**, **Vesia M**, **Yan X**, **Crawford JD**, **Niemeier M.** Parietal area BA7 integrates motor programs for reaching, grasping, and bimanual coordination. *J Neurophysiol* 117: 624–636, 2017. doi:10.1152/jn.00299.2016.
118. **Abedi Khoozani P**, **Blohm G.** Neck muscle spindle noise biases reaches in a multisensory integration task. *J Neurophysiol* 120: 893–909, 2018. doi:10.1152/jn.00643.2017.